Self-Amplified Spontaneous Emission Driven by a High-Brightness Electron Beam

D. C. Nguyen, R. L. Sheffield, C. M. Fortgang, J. C. Goldstein, J. M. Kinross-Wright, and N. A. Ebrahim
Mail Stop H851, Los Alamos National Laboratory, Los Alamos, New Mexico 87545
(Received 12 March 1998)

We report the first high-gain self-amplified spontaneous emission experiment at 15 μm driven by a high-brightness 17-MeV electron beam. A change of two decades in the beam current yields an increase of four decades in the measured infrared power. By fitting the measured infrared pulse energy to an analytic model, we estimate that eight power gain lengths, corresponding to a gain of 300, exist in the wiggler at 279 A. [S0031-9007(98)06692-7]

PACS numbers: 41.60.–m

An electron beam traversing a wiggler emits synchrotron radiation, also called spontaneous emission in analogy to lasers. With sufficient wiggler length and current density, the radiation experiences gain and grows exponentially with distance in the wiggler. This process, known as self-amplified spontaneous emission (SASE), has been extensively explored as a single-pass technique for generating tunable coherent radiation. The interest in SASE results from a strong possibility of producing a picosecond, high-intensity beam of coherent x rays needed for the fourth-generation light source [1].

The one-dimensional (1D) SASE theory was first conceived by Bonifacio *et al.* [2]. Three-dimensional (3D) effects have been treated by Kim [3] and Chin *et al.* [4]. Xie introduced an algorithm for calculating an effective 3D gain length, for a given beam emittance, energy spread, and radiation Rayleigh range, that replaces the 1D gain length in the exponential growth expression [5]. Experimentally, large single-pass gains in the mm-wave region were first reported by Orzechowski *et al.* [6] and later by Kirkpatrick *et al.* [7]. Efforts in extending SASE to shorter wavelengths began with Okuda *et al.* who reported SASE in the 20–40 μm wavelength range [8]. Later, Bocek *et al.* demonstrated SASE at 47 μm with a 4× enhancement over spontaneous emission [9]. Prazeres *et al.* observed SASE at 5–10 μm with a 5× increase over spontaneous emission [10]. Recently, Hogan *et al.* observed a gain of 6 at 16 μm [11] and Babzien *et al.* reported evidence of SASE at 1.06 and 0.63 μm [12]. A question emerges as to whether these recent observations are truly SASE or coherent spontaneous emission (CSE) that arises from sharp longitudinal structures in the electron beam [13]. A demonstration of large gain with the current and wiggler length dependence predicted by SASE is needed to clarify this question.

We report the observation of a SASE gain of 300 at 15.3 μm with the use of high-current, low-emittance electron beams from a photoinjector. The use of the photoinjector electron beam for driving SASE minimizes the gain-reduction effects due to emittance and energy spread. With small electron beam radii and infrared radiation, diffraction is the dominant gain-reduction mechanism, and the output consists of a single transverse guided mode since, in the presence of diffraction, the lowest order mode receives the highest gain [14]. We show that the infrared radiation power measured at a distance from the wiggler evolved from spontaneous emission to SASE as we varied the beam current. We present a simple analytic model that describes such an evolution of radiation power, neglecting slippage effects. We fit the measured infrared energy versus current to the analytic model and obtain the number of gain lengths versus current. From the number of gain lengths, we obtain an estimate of the gain length and compare it with simulations.

The radiated power spectrum of the fundamental guided mode generated by an electron beam at the position z in the wiggler is given by

$$\left.\frac{dP}{d\omega}\right|_z = \left[\left.\frac{dP}{d\omega}\right|_{\text{input}} + \left.\frac{dP}{d\omega}\right|_{\text{noise}}\right] \times \left|\frac{1}{3}\sum_{j=1}^{3} e^{\delta_j 2\rho k_w z}\right|^2, \tag{1}$$

where the terms in the first bracket denote a coherent input and a SASE start-up noise, the terms in the second bracket denote the SASE gain, ρ is the Pierce parameter, k_w is the wiggler wave number, and δ_j denotes the three roots of the cubic dispersion equation, $\delta^3 + i = 0$ [15]. Two of these roots are complex, $\delta = (\pm\sqrt{3}/2 - i/2)$, and correspond to exponentially growing and decaying modes. The third root is imaginary, $\delta = i$, and corresponds to the oscillatory mode. In normal SASE treatments, only the exponentially growing mode is considered. However, when the SASE gain is low as in the low-current cases of our experiment, the correct modeling must include all three roots. Expanding the gain terms of Eq. (1), we obtain

$$\left|\frac{1}{3}\sum_{j=1}^{3} e^{\delta_j 2\rho k_w z}\right|^2 = \frac{1}{9}\left[4\cosh^2(\sqrt{3}\,\rho k_w z) + 4\cosh(\sqrt{3}\,\rho k_w z) \times \cos(3\rho k_w z) + 1\right]. \tag{2}$$

For an axisymmetric electron beam traversing a planar wiggler, the Pierce parameter is given by [5]

$$\rho = \frac{1}{\gamma}\left[\frac{a_w \lambda_w [J_0(\xi) - J_1(\xi)]}{4\sqrt{2}\,\pi\sigma_b}\right]^{2/3}\left(\frac{I}{I_A}\right)^{1/3}, \tag{3}$$

 0031-9007/98/81(4)/810(4)$15.00

where γ is the beam's relativistic factor, a_w is the rms wiggler parameter, $a_w = eB/\sqrt{2}mck_w$, λ_w is the wiggler period, $J_0(\xi)$ and $J_1(\xi)$ are the zeroth-order and first-order Bessel functions, $\xi = a_w^2/[2(1 + a_w^2)]$, I is the peak current, I_A is the Alfvén current ($\sim$17 kA), and σ_b is the rms electron beam radius.

For SASE, the input is zero and the start-up noise is approximated by the spontaneous emission at the end of the first gain length. Yu and Krinsky analyzed the effective noise spectrum and gave the following expression for the case of small electron beams [16]:

$$\left.\frac{dP}{d\omega}\right|_{\text{noise}} \approx \frac{9}{8}\,\pi\theta_w^2 \left.\frac{d^2P}{d\omega\,d\Omega}\right|_{L_g}, \tag{4}$$

where θ_w is the radiation emission angle, $\theta_w^2 = \lambda/L_g$, λ is the radiation wavelength, L_g is the field gain length, $L_g = \lambda_w/2\pi\sqrt{3}\,\rho$, and $\frac{d^2P}{d\omega d\Omega}|_{L_g}$ is the spontaneous power radiated in the forward direction at the first gain length per unit frequency and solid angle. The spontaneous emission power radiated on axis at the resonant frequency by an electron beam traversing N wiggler periods follows a well-known formula [17],

$$\left.\frac{d^2P}{d\omega\,d\Omega}\right|_N = \frac{2N^2 eI\gamma^2 a_w^2[J_0(\xi) - J_1(\xi)]^2}{c(1 + a_w^2)^2 4\pi\varepsilon_0}, \tag{5}$$

where e is the electron charge, c is the velocity of light, and ε_0 is the permittivity of free space. After some algebraic substitutions, we arrive at an expression for the radiation spectrum evaluated on resonance in terms of L_g,

$$\left.\frac{dP}{d\omega}\right|_z = \frac{1}{32}\,\frac{eI}{c\varepsilon_0}\,\frac{a_w^2 L_g[J_0(\xi) - J_1(\xi)]^2}{\lambda_w(1 + a_w^2)} \times \left[4\cosh^2\!\left(\frac{z}{L_g}\right) + 4\cosh\!\left(\frac{z}{L_g}\right)\cos\!\left(\frac{\sqrt{3}\,z}{L_g}\right) + 1\right]. \tag{6}$$

Three-dimensional effects can be included in this expression by using the 3D gain length based on Xie's algorithm [5]. We note that this model does not include slippage which results from the radiation pulse slipping ahead of the electron bunch. Slippage accounts for a reduction in the radiation pulse energy of less than 50%, approximately the ratio of the slippage length (3 ps) to the electron bunch length (6–16 ps).

Experimentally, we measured the infrared pulse energy at the end of the wiggler integrated over all wavelengths. The SASE bandwidth is given by $\frac{\Delta\omega}{\omega}|_{\text{SASE}} = \sqrt{\rho/N_w}$ [3], where ρ is the Pierce parameter ($\rho = 0.021$ at 279 A) and N_w is the number of wiggler periods ($N_w =$ 50 for the 1-m uniform wiggler). The spontaneous emission bandwidth, $\frac{\Delta\omega}{\omega}|_{\text{SE}} = \frac{0.9}{N_w}$, is 1.8% and cannot be differentiated from the SASE bandwidth of 2.0%.

The SASE experimental setup consists of a high-brightness photoinjector integrated into an L-band linac [18], a 2-m-long wiggler [19], electron beam position and temporal diagnostics, and infrared radiation detectors (Fig. 1). The 1300-MHz linac consists of 10.5 cells with a Cs_2Te photocathode in the first half-cell. In operation, the photocathode is illuminated with the quadrupled frequency, 8-ps Gaussian pulses of a mode-locked Nd:YLF laser. The laser consists of a lamp-pumped Nd:YLF oscillator, a fiber-grating compressor, two Nd:YLF amplifiers, LBO, and BBO second-harmonic crystals. The Gaussian UV beam is truncated with a 14-mm diameter circular aperture that is imaged onto the cathode to produce a spatially uniform electron profile. The electron beam's charge was recorded from the intensities of two calibrated beam position monitors before and after the wiggler. Two solenoids, one at the photoinjector and the other 0.4 m in front of the wiggler, are used to match the electron beam into the wiggler. The first solenoid is set to produce an on-axis field of 0.07–0.1 T. The second solenoid is set to produce an on-axis field of 0.5 T that focuses the electron beam at the wiggler entrance.

The plane-polarized wiggler has a 2-cm period in a modified Halbach design [20]. It consists of a 1-m uniform section with an on-axis magnetic field of 0.7 T ($a_w = 0.922$) and a 1-m tapered section. The latter has a 30% linear field taper that is achieved by varying the wiggler gap from 0.59 to 0.95 cm. Each of the 3 cm $\times$ 0.5 cm $\times$ 1.27 cm SmCo magnets is cut with a 0.55 cm $\times$ 0.15 cm rectangular notch. The notched magnets provide nearly equal two-plane focusing with a β function ($\beta = \gamma\lambda_w/\sqrt{2}\,\pi a_w$) of 0.17 m such that a matched 17-MeV electron beam propagates through the wiggler with a constant rms radius ($\sigma = \sqrt{\varepsilon_n\beta/\gamma}$, where ε_n is the rms normalized emittance). Optical transition radiation (OTR), generated by the electron beam impinging on retractable aluminum blades, is used to measure the beam size in the wiggler. The x and y rms radii, measured at four different locations in the wiggler, are within 20% of 0.18 and 0.15 mm, respectively, demonstrating the nearly equal two-plane focusing. From the measured radii and assuming a matched beam, we infer a normalized emittance of 6×10^{-6} m rad at 4.5 nC.

Electron bunch length measurements with a streak camera were performed on OTR light generated by electron beams impinging on a titanium screen before

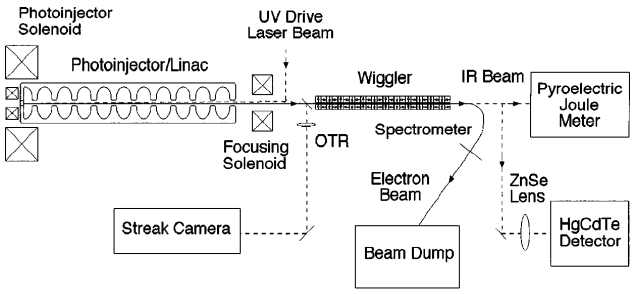

FIG. 1. Experimental setup for self-amplified spontaneous emission driven by a high-brightness, 17-MeV electron beam.

the wiggler. The measured Gaussian bunch lengths were corrected by subtraction in quadrature for the 5.7-ps streak camera resolution. The peak current, defined as the bunch charge divided by the FWHM duration, is plotted versus charge in Fig. 2. Electron beam energy and energy spread are measured with a 120° dipole spectrometer. The measured rms energy spread is 0.33% at 4.5 nC.

The generated infrared radiation was detected with either a calibrated Molectron J50 joule meter or a sensitive HgCdTe detector. Because of physical constraints, the detectors are located 4.5 m from the end of the wiggler (5.5 m from the end of the uniform section). In the energy measurement mode, the infrared light traversed a germanium filter—to eliminate mm-wave radiation—before detection with the joule meter. In the HgCdTe detection mode, the infrared light was focused onto the detector element by a two-inch diameter, $f/2$ ZnSe lens. The SASE spectrum, measured with a 50-line-per-millimeter grating spectrometer, exhibits a central wavelength of 15.3 μm with a FWHM of 0.3 μm.

To determine the dependence of the SASE signal on electron beam current, we varied the charge in each electron bunch by adjusting the UV laser pulse energy on the photocathode. At each bunch charge, we matched the beam into the wiggler by adjusting the solenoid and bucking coil to maximize the SASE signal. As the SASE signal increased, scattering sheets were inserted in front of the detector to keep the signal below saturation. The detector signals were measured before and after each sheet was inserted to determine its attenuation of the SASE signal. At 4.5 nC, we measured an infrared energy, after correction for Fresnel losses in the ZnSe window and Ge filter, of 100 nJ integrated over 500 micropulses. We deduced a pulse energy of 0.2 nJ in each micropulse at 279 A. By comparing the measured HgCdTe signals to that at 4.5 nC, we inferred the SASE pulse energies at different bunch charges. The micropulse energies are plotted versus beam currents in Fig. 3 (circles).

The infrared pulse energy is proportional to the start-up noise integrated over the pulse, which scales with the electron bunch charge Q. As shown in Fig. 2, the peak current follows the relationship $I = Q/(\tau_0 + \alpha Q)$, where τ_0 denotes the shortest bunch length (5.6 ps) and α denotes the space-charge expansion of the electron bunch (2.34 ps/nC). Thus, we can express Q in terms of peak current as $Q = \tau_0 I/(1 - \alpha I)$. The infrared pulse energy, measured at the wiggler exit as a function of current, can be derived from Eq. (6),

$$W(I) = \frac{AI^{2/3}}{(1 - \alpha I)} \times [4\cosh^2(BI^{1/3}) + 4\cosh(BI^{1/3}) \times \cos(B\sqrt{3}\, I^{1/3}) + 1], \qquad (7)$$

where A and B are the fitting coefficients. From the best fit of the measured infrared pulse energy versus current according to Eq. (7) (Fig. 3, solid line), we obtain the number of field gain lengths, the term $BI^{1/3}$, at each beam current. FELEX simulations [21] indicate that the exponential gain decreases sharply after a wiggler length of 1.2 m as the radiation goes out of resonance in the tapered section. Based on these values, we arrive at a scaling law of the field gain length as a function of current for this experiment, $L_g = (0.3m)\,(279A/I)^{1/3}$.

In Table I, we compare the power gain lengths predicted by FELEX [21] and GINGER [22] simulations, and the calculated 3D gain length using Xie's algorithm [5] with experimental observation. The power gain lengths calculated by these three different methods are consistently shorter than the measured value. The radiation mode radius calculated by GINGER simulations at the 1-m location is 350 μm. We believe that diffraction loss

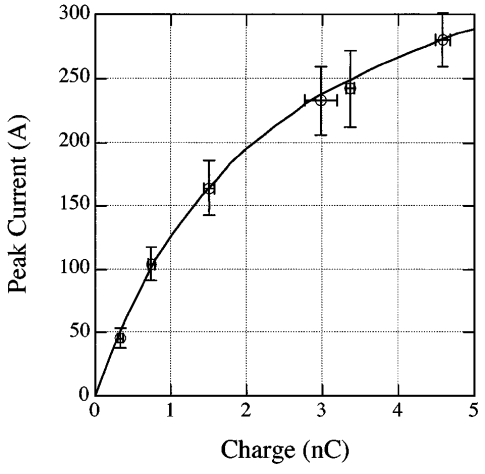

FIG. 2. Plot of electron peak current versus bunch charge. The line is the best fit to the measured bunch charge and lengths, $I/A = 1000(2.34 + 5.6/(Q/nC))^{-1}$.

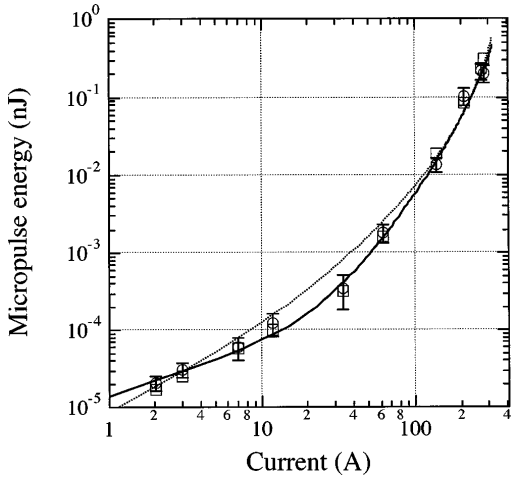

FIG. 3. Log-log plots of measured (circles) and predicted (squares) pulse energy versus current. The solid and dashed lines are least-squares fits to Eq. (7) ($A = 1 \times 10^{-6}$ nJ/A$^{2/3}$; $B = 0.6$ A$^{-1/3}$) and Eq. (8) ($k_1 = 1.06 \times 10^{-3}$ nJ/nC; $k_2 = 9.6$ nC^{-1}), respectively.

TABLE I. Comparison between calculated and measured power gain lengths. The nominal beam parameters are $E = 17$ MeV, $Q = 4.5$ nC, $\tau = 16.1$ ps, $\lambda = 15.3$ μm, $\varepsilon_n = 6$ mm mrad, $\Delta\gamma/\gamma = 0.33\%$, $\lambda_w = 2$ cm, rms $a_w = 0.922$, and betatron period = 1.1 m.

Measurement	FELEX	GINGER	Xie's algorithm
15 cm	8.3 cm	9.6 cm	9.1 cm

inside the tapered wiggler reduces the measured infrared power exiting the wiggler and causes the discrepancy between the measured and calculated gain lengths.

Based on the above gain length scaling law, the measured SASE bandwidth, and the bunch lengths and spot sizes at different beam currents, we calculated the SASE pulse energies using Eq. (6). The calculated SASE pulse energies (Fig. 3, squares) agree well with the measured values (Fig. 3, circles) at all currents, considering that all parameters, except the number of gain lengths, are nonadjustable.

We also checked the hypothesis that the observed signal arises from CSE due to sharp features in the longitudinal electron density distribution. The infrared pulse energy according to the CSE model should scale with Q as follows [23]:

$$W(Q) = k_1 Q(1 + k_2 Q), \tag{8}$$

where k_1 denotes a constant relating spontaneous emission to bunch charge, the second term in the bracket denotes CSE, and k_2 denotes the coherent enhancement. Using the charge-current dependence, we plot the CSE-predicted pulse energy versus current (Fig. 3, dashed line). We note that the SASE model yields a good fit ($\chi^2 = 0.6$, $r^2 = 0.95$), whereas the CSE model ($\chi^2 = 1.1$, $r^2 = 0.92$) does not have sufficient curvature to fit all data points over the entire range of current. We should point out that the CSE prediction based on the most recent current scaling [13] yields an extremely poor fit ($\chi^2 > 3$).

It is difficult to definitively rule out the CSE model based on our data alone, as the above CSE model misses only three data points (Fig. 3). There are, however, two additional observations that argue against the CSE model. First, the CSE signal should not be sensitive to the electron trajectory in the wiggler. In our experiment, a 0.5-mm displacement in either the x or y direction at the last OTR screen reduces the signal by more than a factor of 10, even though the angular displacement of the radiation beam is much smaller than the detector's collection angle. This observation is in disagreement with the CSE model. Second, in a follow-up experiment using the same electron beam with a 2-m-long uniform wiggler with comparable magnetic properties, Hogan *et al.* [24] measured a single-pass gain greater than 10^5. This measurement, combined with our single-pass gain of 300 from the 1-m-uniform and 1-m-tapered wiggler, is inconsistent with the CSE model. The observation of an exponential increase in the single-pass gain with a linear increase in the uniform wiggler length agrees well with the SASE prediction.

We thank B. E. Carlsten, K.-J. Kim, M. Reiser, Y.-C. Chae, S. Anderson, M. E. Weber, and S. K. Volz for their help. This work was performed under the auspices of the U.S. Department of Energy and supported (in part) by funds provided by the University of California for the conduct of discretionary research by Los Alamos National Laboratory.

[1] R. J. Birgeneau and Z. X. Shen, *Report of the BESAC Panel on Synchrotron Radiation Sources and Science* (U.S. Department of Energy, Washington, DC, 1997).
[2] R. Bonifacio, C. Pellegrini, and L. M. Narducci, Opt. Commun. **50**, 373 (1984).
[3] K.-J. Kim, Phys. Rev. Lett. **57**, 1871 (1986).
[4] Y. H. Chin, K.-J. Kim, and M. Xie, Phys. Rev. A **46**, 6662 (1992).
[5] M. Xie, in *Proceedings of the IEEE 1995 Particle Accelerator Conference*, IEEE Cat. No. 95CH35843 (IEEE, Piscataway, NJ, 1995), p. 183.
[6] T. J. Orzechowski *et al.*, Phys. Rev. Lett. **54**, 889 (1985).
[7] D. A. Kirkpatrick *et al.*, Nucl. Instrum. Methods Phys. Res., Sect. A **285**, 43 (1989).
[8] S. Okuda *et al.*, Nucl. Instrum. Methods Phys. Res., Sect. A **331**, 76 (1993).
[9] D. Bocek *et al.*, Nucl. Instrum. Methods Phys. Res., Sect. A **375**, 13 (1996).
[10] R. Prazeres *et al.*, Phys. Rev. Lett. **78**, 2124 (1997).
[11] M. Hogan *et al.*, Phys. Rev. Lett. **80**, 289 (1998).
[12] M. Babzien *et al.*, Phys. Rev. E **57**, 6093 (1998).
[13] J. M. Ortega *et al.*, Phys. Rev. E **57**, 1053 (1998).
[14] G. T. Moore, Opt. Commun. **52**, 46 (1984).
[15] M. Chodorow and C. Susskind, *Fundamentals of Microwave Electronics* (McGraw-Hill, New York, 1964).
[16] L.-H. Yu and S. Krinsky, Nucl. Instrum. Methods Phys. Res., Sect. A **285**, 119 (1989).
[17] B. M. Kincaid, J. Appl. Phys. **48**, 2684 (1977).
[18] R. L. Sheffield, Nucl. Instrum. Methods Phys. Res., Sect. A **393**, 204 (1997).
[19] C. M. Fortgang, Nucl. Instrum. Methods Phys. Res., Sect. A **393**, 385 (1997).
[20] K. Halbach, Nucl. Instrum. Methods Phys. Res., Sect. A **187**, 109 (1981).
[21] B. D. McVey, Nucl. Instrum. Methods Phys. Res., Sect. A **250**, 449 (1986).
[22] R. A. Jong, E. T. Scharlemann, and W. M. Fawley, Nucl. Instrum. Methods Phys. Res., Sect. A **272**, 99 (1988).
[23] D. A. Jaroszynski *et al.*, Phys. Rev. Lett. **71**, 3798 (1993).
[24] M. Hogan *et al.* (to be published).